


Fixed points on band structures of non-Hermitian models: Extended states in the bandgap and ideal superluminal tunneling

Amir M. Jazayeri*

The College of Optics and Photonics (CREOL), University of Central Florida, Orlando, FL, USA
 (Received 10 February 2022; revised 6 March 2023; accepted 21 March 2023; published 6 April 2023)

Space-time reflection symmetry (PT symmetry) in non-Hermitian electronic models has drawn much attention over the past decade mainly because it guarantees that the band structures calculated under open boundary conditions be the same as those calculated under periodic boundary conditions. PT symmetry in electromagnetic (EM) models, which are usually borrowed from electronic models, has also been of immense interest, mainly because it leads to “exceptional” parameter values below which non-Hermitian operators have real eigenvalues, although PT symmetry is not the sole symmetry that allows such exceptional parameter values. In this work, we examine one-dimensional PT-symmetric non-Hermitian EM models to introduce novel concepts and phenomena. We introduce the band-structure concept of “fixed points,” which leads to “bidirectional” reflection zeros in the corresponding finite structures, contrary to a common belief about the EM structures with PT symmetry (and without parity inversion and time-reversal symmetries). Some of the fixed points manifest themselves as, what we name, “extended states in the bandgap” on the band structure while some other fixed points are the “turning points” of the band structure. The extended states in the bandgap are in fact the dual of the well-known “bound states in the continuum,” while the turning points allow us to observe “ideal” superluminal tunneling in the corresponding finite structures. By “ideal” superluminal tunneling, we mean the case where not only the transmission coefficient has an almost uniform phase over a broad bandwidth, but also the magnitudes of the transmission and reflection coefficients are almost equal to unity and zero, respectively, over the bandwidth.

DOI: [10.1103/PhysRevB.107.144302](https://doi.org/10.1103/PhysRevB.107.144302)

I. INTRODUCTION

Spinless electronic systems without time-reversal (T) symmetry are allowed to support protected edge states [1–3] with whose electromagnetic (EM) counterparts can be realized in structures made of materials with a nonreciprocal EM response [4]. Spinful electronic systems with T symmetry are also allowed to support protected edge states [5–7], with EM counterparts that have been realized in structures made of ring resonators [8] and bi-anisotropic elements [9], where the role of spin is played by the EM wave’s propagation direction and polarization, respectively.

Strictly speaking, parity inversion (P) is the reversal of either one spatial coordinate axis or all three spatial coordinate axes. Sometimes the reversal of two spatial coordinate axes is also called parity inversion, although it is in fact a π rotation. Unlike T, which is always non-Hermitian, always antiunitary (leading to $TiT^{-1} = -i$), and sometimes noninvolutory (T^{-1} and T are sometimes different), P (as well as the π rotation operator) is always Hermitian, unitary, and involutory.

The composition of P and T symmetries is especially important in non-Hermitian systems. For instance, the Hermitian Su-Schrieffer-Heeger (SSH) model [10] has two well-known non-Hermitian versions: one that respects PT symmetry [11,12] and the other that does not [11,13]. Non-Hermiticity in the latter, which does *not* respect PT symmetry, completely changes the topological character of the original SSH model

[11,13] and leads to a fundamental difference between the energy spectrum calculated under periodic boundary conditions and the one calculated under open boundary conditions [11,13] *however large* the length of the open sample chosen.

Another well-known consequence of PT symmetry in non-Hermitian systems is that all the eigenvalues of a PT-symmetric non-Hermitian Hamiltonian can be real in a parameter range [14]. The parameter value at which some (or all) of the eigenvalues start to become complex is called an exceptional point. However, we should emphasize that PT symmetry is not the sole symmetry that allows non-Hermitian Hamiltonians to have real eigenvalues. For instance, the non-Hermitian version of the SSH model, which does not respect PT symmetry, *does* have real energy spectra in certain parameter ranges; but, due to lack of PT symmetry, its energy spectrum and exceptional points depend on the choice of boundary conditions.

The PT-symmetric non-Hermitian EM structures reported in the literature are usually borrowed from tight-binding electronic models, and are realized by parallel waveguides weakly coupled to each other, where the role of energy in the electronic models is played *mathematically* by the EM momentum along the waveguides [15–18]. As the correspondence is solely mathematical, a certain *physical* property of such an EM structure does *not* correspond to the *same physical* property of its corresponding electronic model. In particular, the EM band structure, which shows the relationship between the photon’s energy and momentum along the waveguides (or quasi-momentum perpendicular to the waveguides), does *not* correspond to the electronic band structure, which shows

*amir@ucf.edu

the relationship between the electron's energy and quasi-momentum.

The PT-symmetric non-Hermitian EM models to be examined in this work do not have any *tight-binding* electronic counterparts. Furthermore, the regions of EM gain and loss in the to-be-examined EM structures are so thin in comparison with the photon's wavelength that we approximate them by negative and positive surface conductivities, respectively. We can consider the to-be-examined models as "generalized" Kronig-Penney models. Unlike the delta functions in the potential profile of the well-known Kronig-Penney electronic model [19], the delta functions in the permittivity profiles of the to-be-examined EM models are not real-valued and are not necessarily equally spaced. The purpose of this work is to introduce certain novel concepts and phenomena, but it is worth noting that "negative" surface conductivity can, for instance, be realized by using an optically pumped monolayer of graphene and transition-metal dichalcogenides when the EM frequency is in the THz [20,21] and optical range [22], respectively.

II. PT-SYMMETRIC NON-HERMITIAN EM MODELS

A. Revisiting a well-known model and phenomenon

A well-known PT-symmetric EM structure, which was first examined in Ref. [23], is based on a one-dimensional complex refractive index profile $n_b + n_c \cos(2\pi x/\Lambda) + i n_s \sin(2\pi x/\Lambda)$, where n_b , n_c , and n_s are positive numbers at the excitation frequency, and $n_c, n_s \ll n_b$. Let us consider a finite-length structure based on this refractive index profile within $x = 0$ and $x = w \equiv M\Lambda$ in a background of a refractive index n_b , where M is a positive integer. It is evident that such a finite structure is asymmetric when n_s is nonzero, because the left side of the structure starts with a region imposing EM loss while the right side starts with a region yielding EM gain. Let us write the reflected and transmitted electric field phasors as

$$\hat{y}E_0 R_L \exp(-in_b k_0 x) \quad \text{and} \quad \hat{y}E_0 T_{LR} \exp[in_b k_0(x - w)], \quad (1)$$

respectively, when the structure is illuminated from the left (at $x = 0$) by an incident plane wave with the electric field $\hat{y}E_0 \exp(in_b k_0 x)$, and as

$$\hat{y}E_0 R_R \exp[in_b k_0(x - w)] \quad \text{and} \quad \hat{y}E_0 T_{RL} \exp(-in_b k_0 x), \quad (2)$$

respectively, when the structure is illuminated from the right (at $x = w$) by an incident plane wave with the electric field $\hat{y}E_0 \exp[-in_b k_0(x - w)]$. We have denoted the wavenumber in free space by k_0 , which reads ω/c in terms of the speed of light in free space (c) and the excitation angular frequency (ω).

For $n_s = 0$, we know that at the Bragg frequency [when $\omega = \omega_B \equiv \pi c/(n_b \Lambda)$], the structure is a symmetric Bragg mirror, and the reflection coefficients R_L and R_R are equal, and approach unity when $M \rightarrow \infty$. However, for $n_s = n_c$, Kulishov *et al.* [23] observed that at the Bragg frequency, R_L is zero while R_R is an unbounded and increasing function of M . The fact that for any nonzero n_s , the reflection coefficients R_L and R_R are unequal was termed a "nonreciprocal" behavior in Ref. [23], but it should be noted that the structure is in fact

reciprocal (i.e., obeys Lorentz reciprocity), and the transmission coefficients T_{LR} and T_{RL} are always equal. These equal coefficients will hereafter be denoted by T .

The structure was later reexamined by Lin *et al.* [24]. For $n_s = n_c$, they observed [24] that at the Bragg frequency, the magnitude of T is almost unity, and its phase can be approximated by $n_b w \omega/c$ in terms of ω . Therefore, for $n_s = n_c$, the structure is almost "invisible" (i.e., acts as a medium of the refractive index n_b) when it is illuminated from the left by an incident wave packet with a frequency content around the Bragg frequency.

To the best of our knowledge, the structure has only been examined from the scattering-matrix viewpoint in the literature. Therefore, it is worth looking into the band diagram of its underlying periodic refractive index profile [i.e., $n_b + n_c \cos(2\pi x/\Lambda) + i n_s \sin(2\pi x/\Lambda)$, where $n_c, n_s \ll n_b$] so we can later contrast its features with the band diagrams of the EM models to be introduced in this work. However, instead of working with the "refractive index" $n(x)$ defined earlier, we work with the "relative permittivity" $\epsilon(x)$ defined as $\epsilon_b + \epsilon_c \cos(2\pi x/\Lambda) + i \epsilon_s \sin(2\pi x/\Lambda)$, where ϵ_b , ϵ_c , and ϵ_s are positive numbers. The relative permittivity $n^2(x)$ corresponding to the refractive index $n(x)$ is a special case of $\epsilon(x)$ when $\epsilon_c, \epsilon_s \ll \epsilon_b$; in this case, the coefficients of $\epsilon(x)$ can be written as $\epsilon_b = n_b^2$, $\epsilon_c = 2n_b n_c$, and $\epsilon_s = 2n_b n_s$ in terms of the coefficients of $n(x)$. However, by using the standard Fourier expansions of the EM fields [25], we can calculate the band structure of $\epsilon(x)$ without necessarily assuming that $\epsilon_c, \epsilon_s \ll \epsilon_b$.

We only plot the band structure for $0 < k_x < \pi/\Lambda$, because the band structure is symmetric with respect to $k_x = 0$. As is seen in Fig. 1(a), for $\epsilon_s < \epsilon_c$, the band structure has bandgaps. The frequencies located in each bandgap correspond to complex quasi-momentums whose real parts are identical (either zero or π/Λ). The bandgap-center frequencies, at which the imaginary parts of the complex quasi-momentums are maximized, happen at the multiples of the Bragg frequency $\omega_B = \pi c/(\sqrt{\epsilon_b} \Lambda)$ if and only if $\epsilon_c, \epsilon_s \ll \epsilon_b$, because in this case, the sine and cosine parts of $\epsilon(x)$ can be considered small perturbations added to the constant ϵ_b .

As is seen in Fig. 1(b), the bandgaps all narrow when ϵ_s increases, and they all close when ϵ_s becomes equal to ϵ_c . This confirms that $\epsilon_s = \epsilon_c$ is in fact an exceptional parameter value. The band structure for $\epsilon_s = \epsilon_c$ is the same as the band structure for a uniform medium with the relative permittivity ϵ_b . This simply explains the "invisibility" reported in Ref. [24] for a finite structure with ϵ_s equal to ϵ_c and excitation frequencies around ω_B . It is worth noting that the band crossings for $\epsilon_s = \epsilon_c$ all happen at the multiples of ω_B whether ϵ_c is small or not.

As is seen in Fig. 1(c), bandgaps appear again when $\epsilon_s > \epsilon_c$. These bandgaps are in fact thanks to a nonzero ϵ_s and remain open even if $\epsilon_c = 0$. However, a more obvious signature of the spontaneously broken PT symmetry for $\epsilon_s > \epsilon_c$ is the emergence of k-jumps. In the range between any two consecutive bandgaps, the Bloch wave propagating parallel to $+\hat{x}$ (or $-\hat{x}$) has a positive (or negative) k-jump from k_g to $2\pi/\Lambda - k_g$ (or from $2\pi/\Lambda - k_g$ to k_g) at some frequency, where $0 < k_g < \pi/\Lambda$.

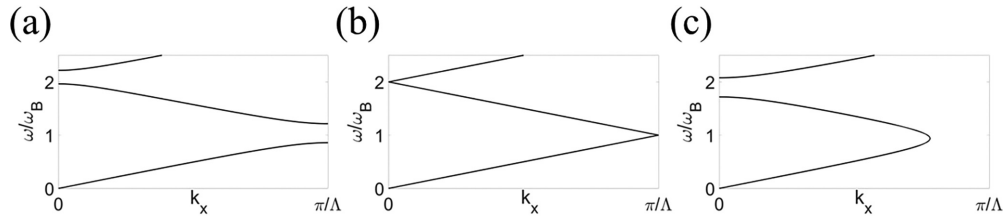


FIG. 1. Band structure of the PT-symmetric relative permittivity profile $\varepsilon_b + \varepsilon_c \cos(2\pi x/\Lambda) + i\varepsilon_s \sin(2\pi x/\Lambda)$ for $\varepsilon_b = 5$, $\varepsilon_c = 4$, and (a) $\varepsilon_s = 2$, (b) $\varepsilon_s = 4$, and (c) $\varepsilon_s = 6$. In (a) and (c), the centers of the bandgaps are not at the multiples of $\omega_B = \pi c/(\sqrt{\varepsilon_b}\Lambda)$ because ε_c and ε_s are not much smaller than ε_b . In (b), the band structure is the same as the band structure of a uniform medium with the relative permittivity ε_b .

B. Novel models, concepts, and phenomena

Let us now focus our attention on the PT-symmetric structures depicted in Fig. 2, each of which consists of surface conductivities σ_S and $-\sigma_S$, a medium of a relative permittivity ε_m , and length $w = M\Lambda$, where the values of σ_S and ε_m are real and positive at the excitation angular frequency ω , M is an integer, and Λ denotes the period of the corresponding infinitely long periodic models. The structures are placed in a background of a positive relative permittivity ε_b . A surface conductivity σ_S at a position $x = a$ is in fact a volume conductivity $\sigma(x)$ in a region so thin in comparison with the photon's wavelength that we approximate $\sigma(x)$ by $\sigma_S\delta(x-a)$, where $\delta(x)$ denotes the Dirac delta function. From an EM viewpoint in the frequency domain, a conductivity σ is in fact equivalent to a complex relative permittivity ε equal to $i\sigma/(\varepsilon_0\omega)$, where the time variation $e^{-i\omega t}$ has been assumed. Positive conductivity (or, equivalently, a positive imaginary part for permittivity) imposes EM loss while negative conductivity (or, equivalently, a negative imaginary part for permittivity) yields EM gain.

Given the geometries of the structures depicted in Fig. 2, we use the standard transfer-matrix method [26] to analyze them at any excitation frequency ω . A transfer matrix is a matrix that relates the EM fields E_y and H_z at a position x_1 to the EM fields at another position x_2 . The scattering-matrix elements [i.e., R_L , R_R , and T , defined in Eqs. (1) and (2)] for each of the structures depicted in Fig. 2 can be built based on the transfer matrix relating the EM fields at $x = 0$ to the EM fields at $x = w \equiv M\Lambda$. We can also use the transfer-matrix method to derive the band structures of the corresponding infinitely long periodic models. For an infinitely long periodic model, the eigenvalues of the transfer matrix relating the EM fields

at $x = x_0 + \Lambda$ to the EM fields at $x = x_0$ can be written as $\exp(ik_x\Lambda)$ in terms of the quasi-momentum k_x corresponding to ω , where x_0 is an arbitrary point that does not coincide with the positions of the surface conductivities. The numerical values of ε_b and ε_m will hereafter be assumed to be equal to 1 and $(1.7)^2$, respectively. Also, we will always normalize ω and σ_S to the Bragg angular frequency (ω_B) and the free-space admittance (Y_0), respectively. It should be noted that, unlike the periodic model examined in the previous subsection, ω_B is now equal to $\pi c/(\sqrt{\varepsilon_m}\Lambda)$ [not $\pi c/(\sqrt{\varepsilon_b}\Lambda)$].

For $\sigma_S = 0$, the EM structure in Fig. 2(a) reduces to a uniform medium of the relative permittivity ε_m . As is seen in Figs. 3(a) and 3(b), the band structure of the corresponding infinitely long periodic model has k -jumps for any nonzero value of σ_S . At any odd multiple of ω_B , the Bloch wave propagating parallel to $+\hat{x}$ (or $-\hat{x}$) has a positive (or negative) k -jump from $-k_G$ to k_G (or from k_G to $-k_G$), where $0 < k_G < \pi/\Lambda$. The k -jumps enlarge and approach $2\pi/\Lambda$ (i.e., k_G increases and approaches π/Λ) when σ_S increases and approaches a threshold σ_{TH} equal to $3.4Y_0$. For $\sigma_S > \sigma_{TH}$, a bandgap covering the whole frequency space, excluding all even multiples of ω_B , appears. For $\sigma_S > \sigma_{TH}$, we name the states corresponding to the even multiples of ω_B “extended states in the bandgap” (ESIBs). These discrete points in the bandgap are in fact “fixed points” of the band structure and appear as Dirac points for $\sigma_S < \sigma_{TH}$. The presence of the fixed points is an important feature that is absent in the band structure examined in Fig. 1.

As the fixed points of the band structure have quasi-momentums equal to π/Λ , we expect the electric field amplitude within the finite structure depicted in Fig. 2(a) to be “fully” periodic regardless of the value of σ_S when it

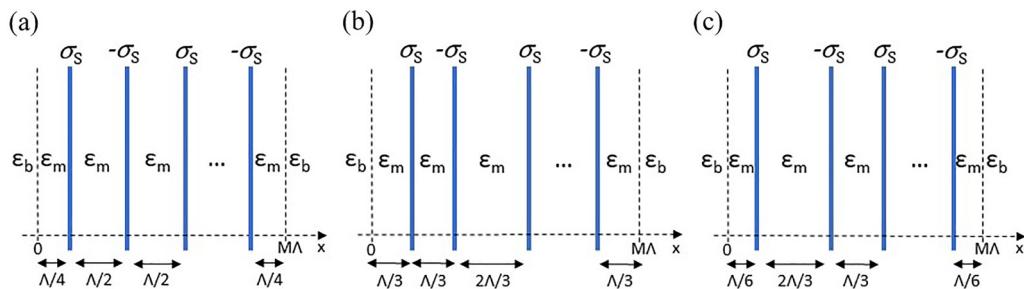


FIG. 2. PT-symmetric EM structures consisting of positive and negative surface conductivities and a medium of a real relative permittivity ε_m and length $w = M\Lambda$, where M is an integer and Λ denotes the period of the corresponding infinitely long periodic models. The structures are placed in a background of a relative permittivity ε_b . The structures in (b) and (c) correspond to one periodic model. For the numerical analysis, we will assume that $\varepsilon_b = 1$, $\varepsilon_m = (1.7)^2$, and $M = 6$.

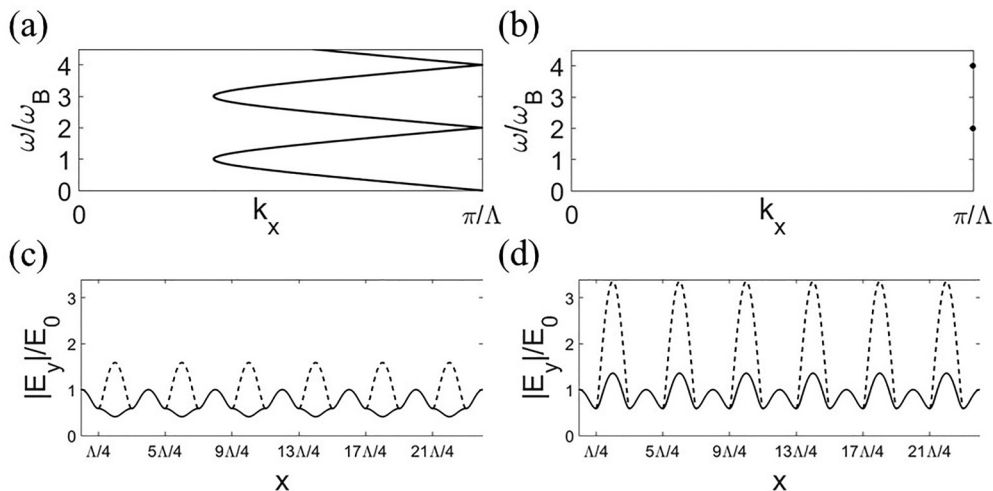


FIG. 3. (a), (b) Band structure of the infinitely long periodic model corresponding to the finite structure in Fig. 2(a) for $\sigma_S = 0.5\sigma_{TH}$ and $\sigma_S = 2\sigma_{TH}$, respectively, where the threshold value σ_{TH} is equal to $3.4Y_0$. The fixed points, which appear as Dirac points for $\sigma_S < \sigma_{TH}$, and ESIBs for $\sigma_S > \sigma_{TH}$, are located at the even multiples of $\omega_B = \pi c/(\sqrt{\epsilon_m}\Lambda)$. (c), (d) Electric field amplitude within the finite structure for $\sigma_S = 0.5\sigma_{TH}$ and $\sigma_S = 2\sigma_{TH}$, respectively, when it is illuminated by a y-polarized plane wave with $\omega = 2\omega_B$ and amplitude E_0 from the left (solid lines) or right (dashed lines).

is illuminated by a plane wave with an angular frequency equal to an even multiple of ω_B . This prediction is confirmed by the numerical results presented in Figs. 3(c) and 3(d). More interestingly, the peak field amplitude within certain regions of the finite structure is fixed and equal to the incident field amplitude regardless of the value of σ_S . Furthermore, as is seen in Figs. 4(a) and 4(b), the reflection coefficient is zero at the even multiples of ω_B regardless of the value of σ_S , whether the structure is illuminated from the left or right. These “bidirectional” reflection zeros contrast with the common belief that the reflection zeros of a structure with PT symmetry (and without P and T symmetries) are unidirectional [27].

The existence of the fixed points at the “even” multiples of ω_B is not the sole interesting feature of the band structure. As is seen in Fig. 3(a), for $\sigma_S < \sigma_{TH}$, the group velocity

$\partial\omega/\partial k_x$ of the Bloch wave propagating parallel to $+\hat{x}$ (or $-\hat{x}$) approaches $+\infty$ (or $-\infty$) when ω approaches any “odd” multiple of ω_B . Therefore, for $\sigma_S < \sigma_{TH}$, we expect a divergent light transmission velocity (i.e., superluminal tunneling) in the finite structure, with excitation frequencies around any “odd” multiple of ω_B . Figure 4(d), which depicts the phase ϕ of the transmission coefficient versus ω , confirms that, for $\sigma_S < \sigma_{TH}$, ϕ is almost uniform around $\omega = \omega_B$, and therefore, the light transmission velocity, defined as $w(\partial\phi/\partial\omega)^{-1}$, diverges around $\omega = \omega_B$. The interesting point about this superluminal tunneling is that the bandwidth over which ϕ is almost uniform becomes very broad and almost equal to ω_B when σ_S increases and approaches σ_{TH} .

Despite the obvious superiority of the superluminal tunneling discussed here over the schemes reported in the literature [28–32], two imperfections still make it nonideal. First, when σ_S is close to σ_{TH} (and therefore the bandwidth of the superluminal tunneling is maximum), none of the reflection coefficients (i.e., neither R_L nor R_R) is close to zero around the odd multiples of ω_B . Second, and more importantly, the magnitude of the transmission coefficient is not close to unity. These two imperfections can be explained based on the band structure of the periodic model. As σ_S increases and approaches σ_{TH} , the states corresponding to the frequencies around any “odd” multiple of ω_B approach “localized” states in the bandgap. Consequently, R_L and R_R depart from zero, and $|T|$ departs from unity when σ_S increases and approaches σ_{TH} . As we will see, these two imperfections are absent in the EM structures depicted in Figs. 2(b) and 2(c).

The two finite structures in Figs. 2(b) and 2(c) correspond to one periodic model. The periodic model reduces to a uniform medium of the relative permittivity ϵ_m when $\sigma_S = 0$. The band structure of the periodic model has been plotted in Fig. 5 for different values of σ_S . For any nonzero value of σ_S smaller than a threshold $\sigma_{TH,1}$ equal to $2.9Y_0$, the band structure has two types of k-jumps. In the case of any k-jump of the first type, the Bloch wave propagating parallel to $+\hat{x}$ (or $-\hat{x}$) has

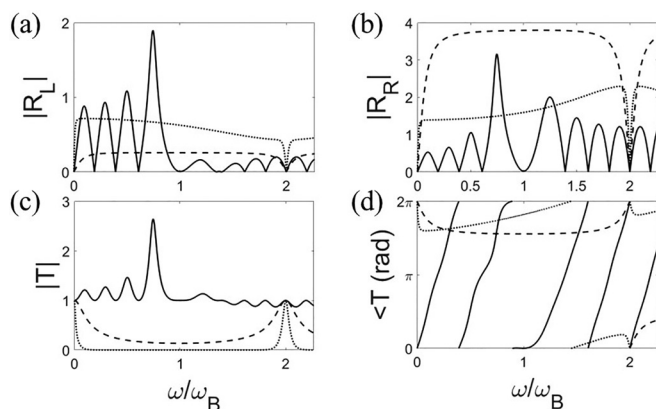


FIG. 4. Frequency response of the (a) magnitude of R_L , (b) magnitude of R_R , (c) magnitude of T , and (d) phase of T for the finite structure in Fig. 2(a) for $\sigma_S = 0.5\sigma_{TH}$ (solid lines), $\sigma_S = \sigma_{TH}$ (dashed lines), and $\sigma_S = 2\sigma_{TH}$ (dotted lines), where the threshold value σ_{TH} is equal to $3.4Y_0$.

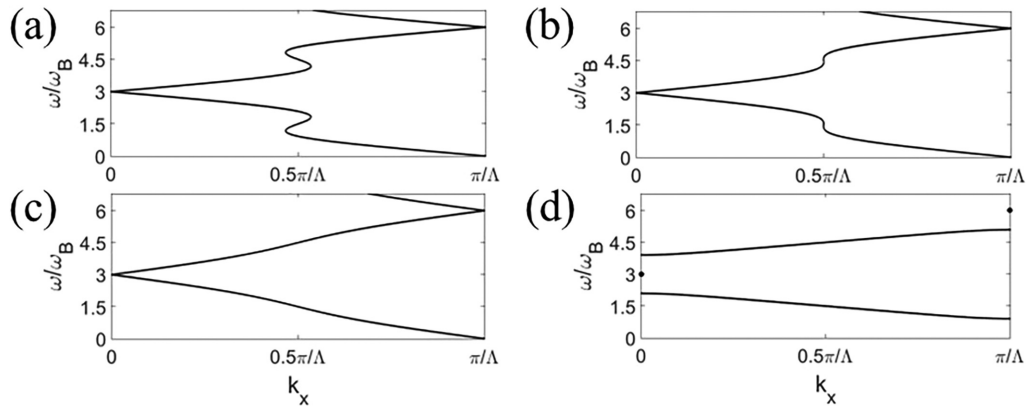


FIG. 5. Band structure of the infinitely long periodic model corresponding to the finite structures in Figs. 2(b) and 2(c) for (a) $\sigma_S < \sigma_{TH,1}$, (b) $\sigma_S = \sigma_{TH,1}$, (c) $\sigma_{TH,1} < \sigma_S < \sigma_{TH,2}$, and (d) $\sigma_{TH,2} < \sigma_S$, where the threshold values $\sigma_{TH,1}$ and $\sigma_{TH,2}$ are equal to $2.9Y_0$ and $3.6Y_0$, respectively. The fixed points located at the multiples of $3\omega_B$ manifest themselves as Dirac points for $\sigma_S < \sigma_{TH,2}$, and as ESIBs for $\sigma_S > \sigma_{TH,2}$. The fixed points located at the odd multiples of $1.5\omega_B$ are the turning points of the band structure.

a positive (or negative) k-jump from $-k_A$ to k_A (or from k_A to $-k_A$), where $0 < k_A < \pi/\Lambda$. In the case of any k-jump of the second type, the Bloch wave propagating parallel to $+\hat{x}$ (or $-\hat{x}$) has a positive (or negative) k-jump from k_B to $2\pi/\Lambda - k_B$ (or from $2\pi/\Lambda - k_B$ to k_B), where $0 < k_B < \pi/\Lambda$. The k-jumps all enlarge and approach π/Λ (i.e., k_A and k_B both increase and approach $0.5\pi/\Lambda$) when σ_S increases and approaches $\sigma_{TH,1}$. However, at the same time, something interesting happens. For the sake of clarity, let us only consider the Bloch waves propagating either parallel to $+\hat{x}$ or $-\hat{x}$. For any k-jump of the first kind with a start point S_A and an end point E_A on the band structure, there is a k-jump of the second type with a start point S_B and an endpoint E_B with the property that E_A and E_B approach S_B and S_A , respectively, when σ_S increases and approaches $\sigma_{TH,1}$. As a result, the two k-jumps make a loop, and cancel out each other when σ_S becomes equal to $\sigma_{TH,1}$. This is why the band structure plotted in Fig. 5 has no k-jumps when σ_S is equal to or larger than $\sigma_{TH,1}$. This feature of the band structure contrasts with the common belief that some or all eigenvalues of a non-Hermitian operator become complex when non-Hermiticity becomes large enough.

The fixed points located at the multiples of $3\omega_B$ on the band structure in Fig. 5 manifest themselves as Dirac points when σ_S is smaller than a threshold $\sigma_{TH,2}$ equal to $3.6Y_0$, and as ESIBs when σ_S becomes larger than $\sigma_{TH,2}$. As is expected, and seen in Figs. 6(a) and 6(b), the electric field amplitude within the finite structure is “fully” periodic regardless of the value of σ_S when it is illuminated by a plane wave at a multiple of $3\omega_B$. Also, the peak field amplitude within certain regions of the finite structure is fixed and equal to the incident field amplitude regardless of the value of σ_S .

Apart from the fixed points corresponding to the multiples of $3\omega_B$ on the band structure, there exist other fixed points that are located at the odd multiples of $1.5\omega_B$ and are in fact the “turning points” of the band structure. The existence of the turning points on the band structure in Fig. 5 is a feature that is absent in the band structure in Figs. 3(a) and 3(b). As the turning points have quasi-momentums equal to $\pm 0.5\pi/\Lambda$, we expect the electric field amplitude within the finite structure to be “fully” periodic regardless of the value of σ_S when it is illuminated by a plane wave with an angular frequency equal to an odd multiple of $1.5\omega_B$. This prediction is confirmed by the numerical results presented in Figs. 6(c) and 6(d).

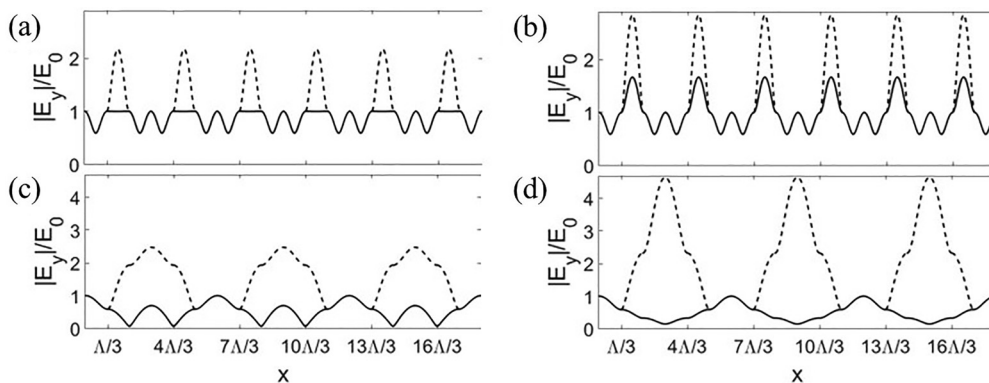


FIG. 6. Electric field amplitude within the finite structure in Fig. 2(b). In (a) and (b), the excitation frequency is equal to $3\omega_B$. In (c) and (d), the excitation frequency is equal to $1.5\omega_B$. In (a) and (c), σ_S is equal to $2.7Y_0$, and is therefore smaller than the threshold value $\sigma_{TH,1}$. In (b) and (d), σ_S is equal to $3.8Y_0$, and therefore larger than the threshold value $\sigma_{TH,2}$. The structure is illuminated by a y-polarized plane wave with amplitude E_0 from the left (solid lines) or right (dashed lines).

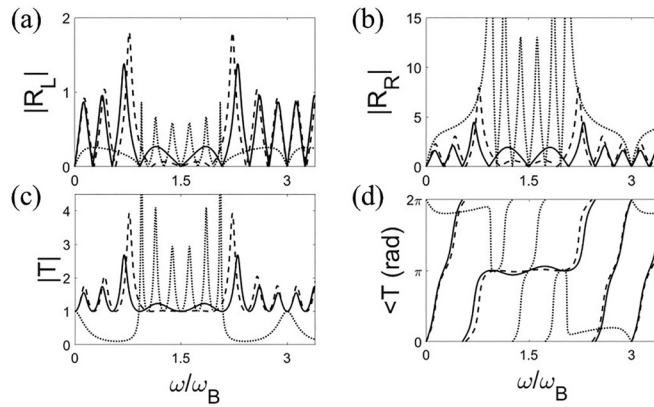


FIG. 7. Frequency response of the (a) magnitude of R_L , (b) magnitude of R_R , (c) magnitude of T , and (d) phase of T for the finite structure in Fig. 2(b). Solid lines are for the case where σ_S is equal to $2.7Y_0$, and therefore smaller than the threshold value $\sigma_{TH,1}$. Dashed lines are for the case where σ_S is almost equal to $\sigma_{TH,1}$. Dotted lines are for the case where σ_S is equal to $3.8Y_0$, and therefore larger than the threshold value $\sigma_{TH,2}$.

As is seen in Figs. 7(a) and 7(b), the reflection coefficient is zero at all the frequencies corresponding to the fixed points (i.e., at all the multiples of $1.5\omega_B$) regardless of the value of σ_S , whether the finite structure is illuminated from the left or right. These “bidirectional” reflection zeros contrast with the common belief about the reflection zeros of PT-symmetric structures [27].

The turning points are especially interesting when σ_S approaches $\sigma_{TH,1}$. At any odd multiple of $1.5\omega_B$, the group velocity of the Bloch wave propagating parallel to $+\hat{x}$ (or $-\hat{x}$) approaches $+\infty$ (or $-\infty$) when σ_S approaches $\sigma_{TH,1}$. Therefore, we expect superluminal tunneling in the finite structure with excitation frequencies around any odd multiple of $1.5\omega_B$ when σ_S approaches $\sigma_{TH,1}$. Figure 7(d) confirms that the phase of the transmission coefficient is almost uniform around $\omega = 1.5\omega_B$ over a very broad bandwidth when σ_S approaches $\sigma_{TH,1}$. This superluminal tunneling is superior to the one discussed earlier for the structure depicted in Fig. 2(a) for two reasons. First, as is seen in Figs. 7(a) and 7(b), the reflection coefficients (i.e., R_L and R_R) are both zero at the odd multiples of $1.5\omega_B$. Second, and more importantly, as is seen in Fig. 7(c), the magnitude of the transmission coefficient is equal to unity at the odd multiples of $1.5\omega_B$. We note that this superluminal tunneling is bidirectional because R_L and R_R are both zero at the odd multiples of $1.5\omega_B$. However, we probably prefer illuminating the structure from the left because R_L remains small over a broad bandwidth around the odd multiples of $1.5\omega_B$.

Finally, we note that the value found for $\sigma_{TH,1}$ by using the band structure of the infinitely long periodic model is almost the same as the value found by using the phase of the

transmission coefficient of the finite structure with six periods (i.e., $M = 6$). However, if we reduce the length of the finite structure, we will see that the two values start to become slightly different.

III. CONCLUDING REMARKS

We introduced the band-structure concept of “fixed points” by examining one-dimensional PT-symmetric non-Hermitian EM models. The fixed points are the points on the band structure that remain intact when a certain parameter value of the model changes.

Two important EM phenomena occur in the finite structures corresponding to the periodic models when the excitation frequency is equal to the eigenfrequency of a fixed point. First, we observe “bidirectional” reflection zeros, which contrast with the common belief that the reflection zeros of structures with PT symmetry (and without P and T symmetries) are unidirectional [27]. Second, the peak field amplitude within certain regions of the finite structures remains fixed and equal to the incident field amplitude, regardless of the parameter value.

Some of the fixed points manifest themselves as what we name ESIBs, which can be considered the dual of the well-known “bound states in the continuum” [33–37]. Similar states in non-Hermitian systems have recently been reported in Ref. [38].

Some other fixed points are in fact the “turning points” of the band structure. The turning points allow us to observe “ideal” superluminal tunneling. It is noteworthy that superluminal tunneling [28–32,39,40] is in fact a combination of two phenomena that do not necessarily accompany each other: tunneling as the energy transmission through barriers [41] and superluminal behavior as unusually small group delays [28–30,42–45]. By “ideal” superluminal tunneling, we specifically refer to the case that is also accompanied by zero reflection and unit transmission over a broad bandwidth. In the cases reported in the literature [28–32], the reflection coefficient is not zero and the magnitude of the transmission coefficient is usually very small.

The band-structure concepts introduced in this work might be useful in designing EM and electronic structures. Quantum-optical treatment of the phenomena reported in this work as well as the inclusion of nonlinear effects remain subjects for future work. Finding the electronic counterparts of the EM structures and phenomena examined here is another interesting problem.

ACKNOWLEDGMENTS

The author is very grateful to Prof. Aristide Dogariu for reviewing the last version of this work and his generous support over the past months. The author is also indebted to Prof. Behzad Rejaei for reviewing the first version of this work and for invaluable discussions in past years.

[1] K. V. Klitzing, G. Dorda, and M. Pepper, New Method for High-Accuracy Determination of the Fine-Structure Constant Based on Quantized Hall Resistance, *Phys. Rev. Lett.* **45**, 494 (1980).

[2] J. Thouless, M. Kohmoto, M. P. Nightingale, and M. den Nijs, Quantized Hall Conductance in a Two-Dimensional Periodic Potential, *Phys. Rev. Lett.* **49**, 405 (1982).

- [3] F. D. M. Haldane, Model for a Quantum Hall Effect without Landau Levels: Condensed-Matter Realization of the Parity Anomaly, *Phys. Rev. Lett.* **61**, 2015 (1988).
- [4] Z. Wang, Y. D. Chong, J. D. Joannopoulos, and M. Soljačić, Reflection-Free One-Way Edge Modes in a Gyromagnetic Photonic Crystal, *Phys. Rev. Lett.* **100**, 013905 (2008).
- [5] C. L. Kane and E. J. Mele, Quantum Spin Hall Effect in Graphene, *Phys. Rev. Lett.* **95**, 226801 (2005).
- [6] B. A. Bernevig, T. L. Hughes, and S. C. Zhang, Quantum spin Hall effect and topological phase transition in HgTe quantum wells, *Science* **314**, 1757 (2006).
- [7] M. König, S. Wiedmann, C. Brune, A. Roth, H. Buhmann, L. W. Molenkamp, X. L. Qi, and S. C. Zhang, Quantum spin Hall insulator state in HgTe quantum wells, *Science* **318**, 766 (2007).
- [8] M. Hafezi, S. Mittal, J. Fan, A. Migdall, and J. M. Taylor, Imaging topological edge states in silicon photonics, *Nat. Photonics* **7**, 1001 (2013).
- [9] B. Khanikaev, S. H. Mousavi, W. K. Tse, M. Kargarian, A. H. MacDonald, and G. Shvets, Photonic topological insulators, *Nat. Mater.* **12**, 233 (2013).
- [10] W. P. Su, J. R. Schrieffer, and A. J. Heeger, Solitons in Polyacetylene, *Phys. Rev. Lett.* **42**, 1698 (1979).
- [11] F. K. Kunst, E. Edvardsson, J. C. Budich, and E. J. Bergholtz, Biorthogonal Bulk-Boundary Correspondence in Non-Hermitian Systems, *Phys. Rev. Lett.* **121**, 026808 (2018).
- [12] W. Song, W. Sun, C. Chen, Q. Song, S. Xiao, S. Zhu, and T. Li, Breakup and Recovery of Topological Zero Modes in Finite Non-Hermitian Optical Lattices, *Phys. Rev. Lett.* **123**, 165701 (2019).
- [13] S. Yao and Z. Wang, Edge States and Topological Invariants of Non-Hermitian Systems, *Phys. Rev. Lett.* **121**, 086803 (2018).
- [14] C. M. Bender and S. Boettcher, Real Spectra in Non-Hermitian Hamiltonians Having PT Symmetry, *Phys. Rev. Lett.* **80**, 5243 (1998).
- [15] H. Schomerus, Topologically protected midgap states in complex photonic lattices, *Opt. Lett.* **38**, 1912 (2013).
- [16] S. Weimann, M. Kremer, Y. Plotnik, Y. Lumer, S. Nolte, K. G. Makris, M. Segev, M. C. Rechtsman, and A. Szameit, Topologically protected bound states in photonic parity-time-symmetric crystals, *Nat. Mater.* **16**, 433 (2017).
- [17] S. Ke, D. Zhao, J. Liu, Q. Liu, Q. Liao, B. Wang, and P. Lu, Topological bound modes in anti-PT-symmetric optical waveguide arrays, *Opt. Exp.* **27**, 13858 (2019).
- [18] S. K. Özdemir, S. Rotter, F. Nori, and L. Yang, Parity-time symmetry and exceptional points in photonics, *Nat. Mater.* **18**, 783 (2019).
- [19] R. de L. Kronig and W. G. Penney, Quantum mechanics of electrons in crystal lattices, *Proc. R. Soc. London A* **130**, 499 (1931).
- [20] M. Sakhdari, M. Farhat, and P. Y. Chen, PT-symmetric metasurfaces: Wave manipulation and sensing using singular points, *New J. Phys.* **19**, 065002 (2017).
- [21] M. Farhat, M. Yang, Z. Ye, and P. Y. Chen, PT-symmetric absorber-laser enables electromagnetic sensors with unprecedented sensitivity, *ACS Photonics* **7**, 2080 (2020).
- [22] S. Buddhiraju, A. Song, G. T. Papadakis, and S. Fan, Nonreciprocal Metamaterial Obeying Time-Reversal Symmetry, *Phys. Rev. Lett.* **124**, 257403 (2020).
- [23] M. Kulishov, J. M. Laniel, N. Bélanger, J. Azaña, and D. V. Plant, Nonreciprocal waveguide Bragg gratings, *Opt. Exp.* **13**, 3068 (2005).
- [24] Z. Lin, H. Ramezani, T. Eichelkraut, T. Kottos, H. Cao, and D. N. Christodoulides, Unidirectional Invisibility Induced by PT-Symmetric Periodic Structures, *Phys. Rev. Lett.* **106**, 213901 (2011).
- [25] K. Sakoda, *Optical Properties of Photonic Crystals* (Springer, New York, 2004).
- [26] M. Born and E. Wolf, *Principles of Optics: Electromagnetic Theory of Propagation, Interference and Diffraction of Light* (Cambridge University Press, Cambridge, 2002).
- [27] D. Stone, W. R. Sweeney, C. W. Hsu, K. Wisal, and Z. Wang, Reflectionless excitation of arbitrary photonic structures: A general theory, *Nanophotonics* **10**, 343 (2021).
- [28] C. Spielmann, R. Szipöcs, A. Stingl, and F. Krausz, Tunneling of Optical Pulses Through Photonic Band Gaps, *Phys. Rev. Lett.* **73**, 2308 (1994).
- [29] S. Longhi, M. Marano, P. Laporta, and M. Belmonte, Superluminal optical pulse propagation at 1.5 μm in periodic fiber Bragg gratings, *Phys. Rev. E* **64**, 055602(R) (2001).
- [30] S. Manipatruni, P. Dong, Q. Xu, and M. Lipson, Tunable superluminal propagation on a silicon microchip, *Opt. Lett.* **33**, 2928 (2008).
- [31] H. G. Winful, Nature of Superluminal Barrier Tunneling, *Phys. Rev. Lett.* **90**, 023901 (2003).
- [32] M. Büttiker and S. Washburn, Ado about nothing much? *Nature (London)* **422**, 271 (2003).
- [33] C. W. Hsu, B. Zhen, A. D. Stone, J. D. Joannopoulos, and M. Soljačić, Bound states in the continuum, *Nat. Rev. Mater.* **1**, 16048 (2016).
- [34] S. Longhi, Bound states in the continuum in PT-symmetric optical lattices, *Opt. Lett.* **39**, 1697 (2014).
- [35] Y. Kartashov, C. Milián, V. V. Konotop, and L. Torner, Bound states in the continuum in a two-dimensional PT-symmetric system, *Opt. Lett.* **43**, 575 (2018).
- [36] Q. Song, J. Hu, S. Dai, C. Zheng, D. Han, J. Zi, Z. Q. Zhang, and C. T. Chan, Coexistence of a new type of bound state in the continuum and a lasing threshold mode induced by PT symmetry, *Sci. Adv.* **6**, eabc1160 (2020).
- [37] D. V. Novitsky, A. S. Shalin, D. Redka, V. Bobrovs, and A. V. Novitsky, Quasibound states in the continuum induced by PT symmetry breaking, *Phys. Rev. B* **104**, 085126 (2021).
- [38] W. Wang, X. Wang, and G. Ma, Extended State in a Localized Continuum, *Phys. Rev. Lett.* **129**, 264301 (2022).
- [39] R. Y. Chiao, P. G. Kwiat, and A. M. Steinberg, Faster than light? *Sci. Am.* **269**, 52 (1993).
- [40] H. G. Winful, Tunneling time, the Hartman effect, and superluminality: A proposed resolution of an old paradox, *Phys. Rep.* **436**, 1 (2006).
- [41] Y. Liu, F. Sun, Y. Yang, Z. Chen, J. Zhang, S. He, and Y. Ma, Broadband Electromagnetic Wave Tunneling with Transmuted Material Singularity, *Phys. Rev. Lett.* **125**, 207401 (2020).

- [42] P. A. Gusikhin, V. M. Muravev, and I. V. Kukushkin, Superluminal electromagnetic two-dimensional plasma waves, *Phys. Rev. B* **102**, 121404(R) (2020).
- [43] T. Low, P. Y. Chen, and D. N. Basov, Superluminal plasmons with resonant gain in population inverted bilayer graphene, *Phys. Rev. B* **98**, 041403(R) (2018).
- [44] L. J. Wang, A. Kuzmich, and A. Dogariu, Gain-assisted superluminal light propagation, *Nature (London)* **406**, 277 (2000).
- [45] Q. Li, T. Wang, Y. Su, M. Yan, and M. Qiu, Coupled mode theory analysis of mode-splitting in coupled cavity system, *Opt. Exp.* **18**, 8367 (2010).